Observation of Incipient Charge Nematicity in $Ba(Fe_{1-X}Co_X)_2As_2$

Y. Gallais,[1,*] R. M. Fernandes,[2] I. Paul,[1] L. Chauvière,[1] Y.-X. Yang,[1] M.-A. Méasson,[1] M. Cazayous,[1] A. Sacuto,[1] D. Colson,[3] and A. Forget[3]

[1]*Laboratoire Matériaux et Phénomenes Quantiques (UMR 7162 CNRS), Université Paris Diderot-Paris 7, Bâtiment Condorcet, 75205 Paris Cedex 13, France*

[2]*School of Physics and Astronomy, University of Minnesota, Minneapolis, Minnesota 55455, USA*

[3]*CEA-Saclay, IRAMIS, Service de Physique de l'Etat Condensé (SPEC URA CNRS 2464), F-91191 Gif-sur-Yvette, France*

(Received 19 June 2013; published 27 December 2013)

Using electronic Raman spectroscopy, we report direct measurements of charge nematic fluctuations in the tetragonal phase of *strain-free* $Ba(Fe_{1-x}Co_x)_2As_2$ single crystals. The strong enhancement of the Raman response at low temperatures unveils an underlying charge nematic state that extends to superconducting compositions and which has hitherto remained unnoticed. Comparison between the extracted charge nematic susceptibility and the elastic modulus allows us to disentangle the charge contribution to the nematic instability, and to show that charge nematic fluctuations are weakly coupled to the lattice.

DOI: 10.1103/PhysRevLett.111.267001 PACS numbers: 74.70.Xa, 74.25.nd

Electronic analogues of nematic states, in which rotational symmetry is broken but translational invariance is preserved, have been proposed in a variety of correlated materials [1], such as quantum Hall systems [2], cuprates [3,4], ruthenates [5], heavy fermions [6] and, more recently, iron pnictide superconductors [7,8]. In the latter, several experiments [7,9–13] on strained samples have collected strong but indirect evidence that the tetragonal-to-orthorhombic structural transition is driven not by the lattice, but by electronic nematicity. However, these measurements could not disentangle the roles of the spin [14–17], charge, and orbital [18–21] degrees of freedom in the nematic instability.

In $Ba(Fe_{1-x}Co_x)_2As_2$, the structural transition at T_s either precedes or accompanies a magnetic transition at T_N, disappearing near the doping concentration with the highest superconducting transition temperature T_c [see the phase diagram of Fig. 1(a)]. The nematic or orthorhombic state is characterized by inequivalent Fe-Fe bond lengths along the in-plane a and b directions [x and y coordinates, respectively, of the one-Fe unit cell used throughout, see Fig. 1(a)], and by anisotropic electronic properties [7,9,12,13,22]. If this state is indeed a consequence of the condensation of an electronic nematic order parameter, its fluctuations should be present in the tetragonal phase and should increase as the temperature is lowered towards T_s. Probing these electronic nematic fluctuations directly is therefore fundamental to unveil the nature of the structural transition, and to evaluate their possible role in the superconducting pairing mechanism.

Here, we report electronic Raman scattering measurements of the charge nematic susceptibility in the tetragonal phase of $Ba(Fe_{1-x}Co_x)_2As_2$ single crystals in which no explicit tetragonal symmetry breaking stress was applied (i.e., strain-free crystals). We show that charge nematic fluctuations are manifested in the Raman spectra by a quasielastic peak in the x^2-y^2 (B_{1g}) symmetry, whose intensity strongly increases in the tetragonal phase upon approaching T_s, signaling an incipient charge nematic order. The extracted static charge nematic susceptibility displays a sizable enhancement over a wide doping range above the superconducting dome, suggesting it may play a role in the superconducting mechanism. Comparison with available shear modulus data indicates that the enhanced charge nematic susceptibility is weakly coupled to the lattice, highlighting the need to incorporate additional degrees of freedom to explain the structural transition.

Raman experiments have been carried out using a diode-pumped solid state laser emitting at 532 nm and a triple grating spectrometer equipped with a nitrogen cooled CCD camera [24]. Single crystals of $Ba(Fe_{1-x}Co_x)_2As_2$ were grown using the self-flux method. The magnetic and superconducting transition temperatures were determined by transport measurements performed on crystals from the same batch [26]. The structural transition temperature was determined by monitoring phonon anomalies observed when entering the orthorhombic phase [25].

The electronic Raman response, χ^μ, probes the weighted charge correlation function $\langle\rho^\mu(\omega)\rho^\mu(-\omega)\rangle$, where $\rho^\mu = \sum_{\mathbf{k}}\gamma^\mu_{\mathbf{k}}n_{\mathbf{k}}$ depends on the charge-density operator $n_{\mathbf{k}}$ of the momentum state $\mathbf{k}$, and on the form factor $\gamma^\mu_{\mathbf{k}}$ whose symmetry μ is determined by the polarizations $\mathbf{e}_I$ and $\mathbf{e}_S$ of the incident and scattered photons [27,23]. To probe the in-plane charge nematic fluctuations, two polarization configurations can be considered [see inset of Fig. 1(d)]. For photons polarized along the diagonals of the Fe-Fe bonds, the form factor has x^2-y^2 (B_{1g}) symmetry, and is sensitive to nematic order along the Fe-Fe bonds. This is the type of C_4 (tetragonal) symmetry-breaking realized in the iron pnictides.

Note that while the charge nematic order parameter $\phi_{\mathbf{k}} \propto \gamma_{\mathbf{k}}^{x^2-y^2} n_{\mathbf{k}}$ changes sign under a 90° rotation, χ^{μ} is proportional to its square $\varphi_{\mathbf{k}}^2$ and therefore is C_4 symmetric. Thus, unlike previous transport anisotropy measurements [7,9,11], we can extract the nematic fluctuations directly from the Raman response without applying any external symmetry-breaking field such as uniaxial stress. Besides the x^2-y^2 (B_{1g}) symmetry, we also investigated the form factor with xy (B_{2g}) symmetry, which is insensitive to changes that make x and y inequivalent. The behaviors of these form factors in momentum space are depicted in Fig. 1(c).

Because of the fluctuation-dissipation theorem, the dynamic charge nematic fluctuations should be manifested in the imaginary part of the Raman response function $(\chi^{\mu})''$ in the appropriate symmetry μ, namely, the x^2-y^2 (B_{1g}) symmetry [28,29]. This is illustrated in Fig. 1(d) for a strain-free, single crystal of the parent compound $BaFe_2As_2$, where $(\chi^{\mu})''$ is plotted as function of frequency

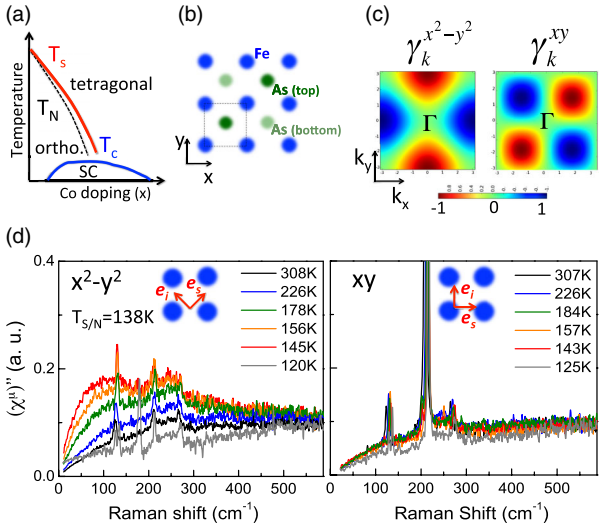

FIG. 1 (color online). (a) Sketch of the phase diagram of $Ba(Fe_{1-x}Co_x)_2As_2$. T_s, T_N, and T_c are the structural, magnetic, and superconducting (SC) transition temperatures, respectively. (b) Tetragonal FeAs layer, with the x and y axes defined along the Fe-Fe bonds. (c) Momentum-space structure of the form factor $\gamma_{\mathbf{k}}^{\mu}$ for x^2-y^2 and xy symmetries [23]. (d) Temperature dependent Raman response $(\chi^{x^2-y^2})''$ and $(\chi^{xy})''$ in a strain-free $BaFe_2As_2$ single crystal with $T_s = 138$ K. The incoming and outgoing photon polarizations (e_I ,e_S) used for each symmetry configuration are depicted in the insets. The sharp peaks are due to phonon excitations. The electronic Raman continuum in x^2-y^2 symmetry displays a low frequency quasielastic peak (QEP) that is superimposed on a weaker and broad continuum that extends to energies above 1000 cm^{-1} and is essentially temperature independent in the tetragonal phase (see Supplemental Material [24]). In the orthorhombic phase, this broad continuum shows a suppression below 500 cm^{-1} in both symmetries because of the Fermi surface reconstruction induced by the simultaneous magnetic order [25].

for different temperatures and for the two symmetries described above. While the response in the xy symmetry is essentially temperature independent above $T_s = 138$ K, the x^2-y^2 response displays a considerable buildup of intensity below 500 cm^{-1} upon approaching T_s, with a subsequent collapse in the nematic or orthorhombic phase. The temperature dependence and the distinctive x^2-y^2 symmetry of this low frequency quasielastic peak (QEP) clearly links it to dynamic charge nematic fluctuations corresponding to an orientational order along the Fe-Fe bonds. While the spectral line shape of the QEP is linked to the relaxational dynamics of the nematic fluctuations [30], we choose here to concentrate on a more transparent quantity: the static charge nematic susceptibility. Indeed the strong increase of the QEP intensity is associated with an enhanced static charge nematic susceptibility, $\chi_0^{x^2-y^2}$, via the Kramers-Kronig relation:

$$\chi_0^{x^2-y^2} = \frac{2}{\pi}\int_0^{\infty} d\omega (\chi'')^{x^2-y^2}(\omega)/\omega. \quad (1)$$

The relevant quantity governing the static nematic susceptibility is thus the Raman conductivity χ''/ω, highlighting the importance of the low frequency part of χ'' in determining $\chi_0^{x^2-y^2}$. The temperature dependence of χ''/ω, where the QEP is now centered at zero frequency, is shown in Fig. 2(a) for six different Co concentrations of $Ba(Fe_{1-x}Co_x)_2As_2$, spanning the phase diagram from the parent $x = 0$ composition ($T_s = 138$ K and $T_c = 0$) up to the strongly overdoped $x = 0.20$ composition ($T_s = T_c = 0$). For $x \leq 0.045$, the QEP displays a systematic enhancement as temperature is lowered towards T_s before collapsing in the symmetry broken phase. The enhancement of the QEP extends down to T_c for $x = 0.065$ where the superconducting transition temperature is optimal and no structural transition is detected. For this particular composition the QEP was found to disappear quickly upon entering the superconducting state indicating a suppression of nematic fluctuations in the superconducting state (not shown). Above optimal composition, the enhancement of the QEP is strongly reduced but remains sizable even for $x = 0.10$, before disappearing for $x = 0.20$. The static charge nematic susceptibility $\chi_0^{x^2-y^2}$ was extracted using Eq. (1) via a partial integration of the Raman conductivity up to 500 cm^{-1}, since above this frequency the spectra are temperature independent in the tetragonal phase. To perform the integration, we used a Lorentzian relaxational form to extrapolate the Raman conductivity spectra from the lowest frequency experimentally accessible, 9 cm^{-1}, down to zero [24]. The doping and temperature dependence of $\chi_0^{x^2-y^2}$ are summarized in the phase diagram of Fig. 2(b). The maximum of the static charge nematic susceptibility closely tracks the structural transition temperature in the underdoped region, vanishing near optimal doping. This temperature and doping dependence

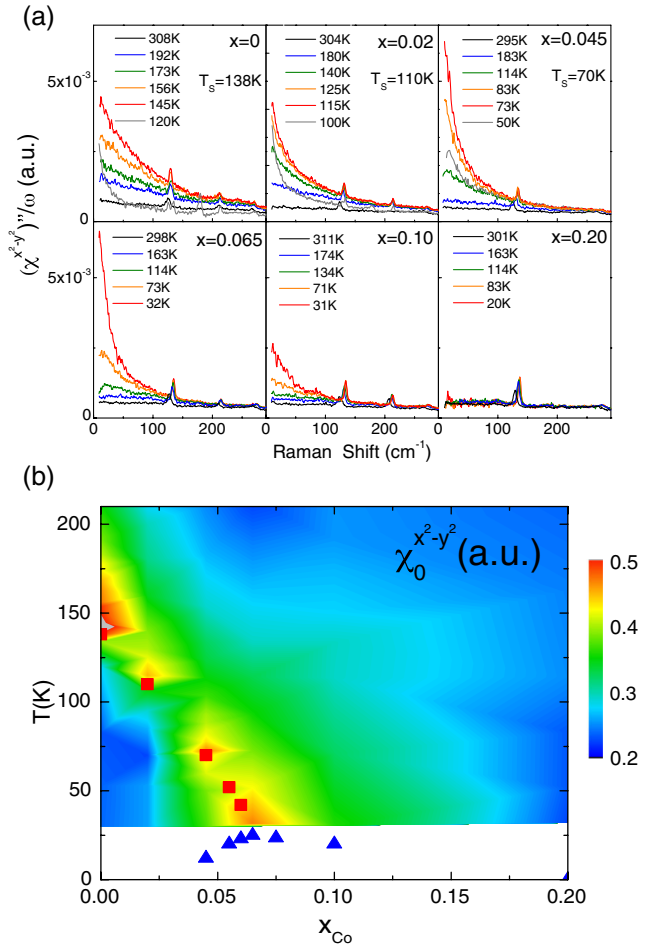

FIG. 2 (color online). (a) Temperature dependent Raman conductivity $(\chi^{x^2-y^2})''/\omega$ for $x = 0$ (parent), $x = 0.02$ (strongly underdoped), $x = 0.045$ (underdoped), $x = 0.065$ (optimally doped), $x = 0.10$ (overdoped), and $x = 0.20$ (strongly overdoped). The structural transition temperature is indicated for the three underdoped compositions. The $x = 0.065$ composition corresponds to optimal superconducting transition temperature ($T_c = 24.5$ K where no structural transition was detected. (b) Evolution of the static charge nematic susceptibility, $\chi_0^{x^2-y^2}$, as a function of temperature and doping. The structural transition temperature T_s and the superconducting transition temperature T_c are indicated in red squares and blue triangles, respectively.

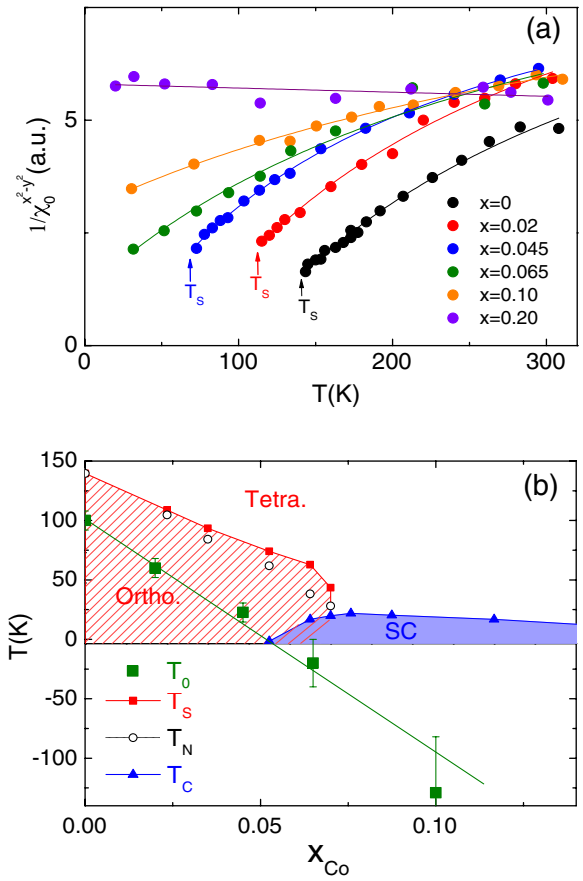

FIG. 3 (color online). (a) Temperature dependence of the inverse nematic charge susceptibility, $(\chi_0^{x^2-y^2})^{-1}$, in the tetragonal phase ($T > T_s$) as a function of Co composition. The lines are Curie-Weiss fits for each composition (see text). (b) (x, T) phase diagram showing the orthorhombic (Ortho) and superconducting (SC) phases. The mean-field transition temperature extracted from the Curie-Weiss fit, T_0, is shown as green squares (the green line is a linear fit of its doping dependence). The corresponding structural transition temperature T_s (red squares), magnetic transition temperature T_N (white circles), and superconducting transition temperature T_c (blue triangles) are also indicated [26].

is qualitatively consistent with previous anistropic transport data of strained crystals [7,9,11]. However, resistivity anisotropy is only an indirect probe of the nematic order parameter since it cannot disentangle the various possible sources of electronic nematicity.

To perform a more quantitative analysis, in Fig. 3(a) we plot the inverse susceptibility as a function of temperature in the tetragonal phase ($T > T_s$) and for the six Co compositions. The softening of the inverse susceptibility, is seen for all compositions up to $x = 0.10$, being absent only for the strongly overdoped, nonsuperconducting, $x = 0.20$ composition. For all other compositions the inverse susceptibility above T_s can be well described over a large temperature range, spanning at least 150 K, by a simple Curie-Weiss law of the form

$$(\chi_0^{x^2-y^2})^{-1}(T) = \left(A + \frac{C}{T - T_0}\right)^{-1}, \qquad (2)$$

where A and C are constants and T_0 is the charge nematic transition temperature. The resulting fits for the inverse susceptibility are shown in Fig. 3(a). They unveil an incipient charge nematic instability at T_0 over a wide doping range, which includes the superconducting dome, in the phase diagram of $Ba(Fe_{1-x}Co_x)_2As_2$.

The extracted T_0 follows the trend of the thermodynamic structural transition temperature T_s, decreasing with doping and vanishing near $x \sim 0.06$. However, T_0 is significantly

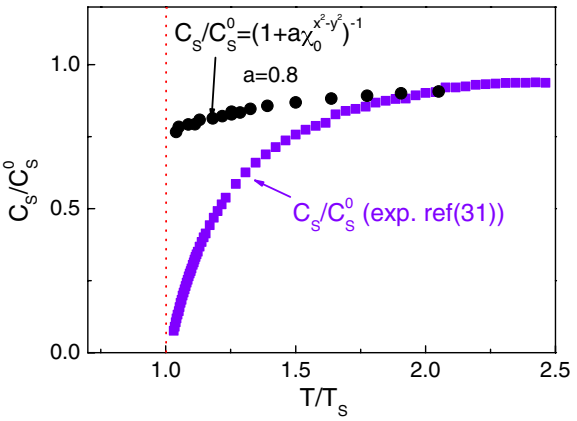

FIG. 4 (color online). Temperature dependence of the experimental shear modulus (data of Ref. [31], in purple), together with the expected temperature dependence of the shear modulus due to the coupling between the charge nematic and orthorhombic order parameters using Eq. (3) (in black). The bare shear modulus was assumed to be temperature independent and the only adjustable parameter, $a = \lambda^2/C_S^0$ (see text) was chosen to fit the shear modulus data at high temperatures ($a = 0.8$). The temperature scale was normalized using the measured structural transition temperatures ($T_S = 130$ K in Ref. [31]).

smaller than T_s, by about 50 K, across the entire phase diagram [see Fig. 3(b)]. This fact, in conjunction with the observation of the buildup of the charge nematic fluctuations over a large temperature range, allow us to conclude that the incipient charge nematicity is not a mere consequence of the softening of the lattice orthorhombicity via a static linear coupling. More importantly, since the Curie-Weiss expression (2) with T_0 significantly smaller than T_s describes very well the data up to a few Kelvin above T_s, it implies that the incipient charge nematicity is, in fact, weakly coupled to the lattice. Because the tetragonal symmetry breaking has to occur at the same temperature in both elastic and charge degrees of freedom, our analysis thus suggests the presence of another nematic degree of freedom which drives the structural transition at T_s.

We can also draw the same conclusions simply by comparing the $\chi_0^{x^2-y^2}$ data directly with the shear modulus $C_s \equiv C_{11} - C_{12}$, which measures the orthorhombic lattice stiffness [31,32]. Since, by symmetry, the order parameters associated with C_s and $\chi_0^{x^2-y^2}$ are linearly coupled, we obtain

$$\frac{C_S}{C_S^0} = \left[1 + \left(\frac{\lambda^2}{C_S^0}\right)\chi_0^{x^2-y^2}\right]^{-1}, \qquad (3)$$

provided charge nematicity is the only soft mode present [17,31]. Here, λ is the linear coupling constant and C_s^0 is the high-temperature shear modulus. In Fig. 4, we test the validity of the above relation for the parent compound $BaFe_2As_2$ by comparing the C_s values inferred from our $\chi_0^{x^2-y^2}$ data via Eq. (3) (black) with the experimental C_s data of Ref. [31] (purple). The discrepancy between the two confirms our inference above that charge nematicity is not the only soft mode, suggesting the presence of an additional electronic nematic degree of freedom. The precise nature of this additional degree of freedom cannot be ascertained from our Raman study. It is possible that spin fluctuations drive the softening of C_s [14–17] and $\chi_0^{x^2-y^2}$ via spin-lattice and spin-charge couplings, respectively. Alternatively, it has also been proposed that the structural transition is driven by orbital ordering between xz and yz Fe $3d$ orbitals [18–21]. Although the charge fluctuations measured here do not necessarily come only from fluctuations of the relative charge $n_{xz} - n_{yz}$ between these two orbitals, it follows from the orbital content of the Fermi surface of the iron pnictides that these orbital fluctuations should give a major contribution to $\chi_0^{x^2-y^2}$ if orbital order is the driving instability ([33], see also Supplemental Material [34]).

In conclusion, we presented electronic Raman spectroscopy study of $Ba(Fe_{1-x}Co_x)_2As_2$ single crystals in the tetragonal phase, where the C_4 symmetry is intact. Our analysis of the temperature dependence of the enhanced charge nematic susceptibility, and its comparison to the shear modulus data, indicate that although these fluctuations contribute to promote the breaking of the tetragonal symmetry, they are not the only driving mechanism behind it. The persistence of these fluctuations above the entire superconducting dome raises the question of whether they play a role in the pairing mechanism [22,35]. Our results are reminiscent of earlier Raman studies indicating fingerprints of fluctuating charge density wave order in cuprates [28,36]. We note, however, that in contrast to the stripe or checkerboard orders observed in cuprates, the fluctuating nematic order observed here does not break any lattice translational symmetry. Besides shedding light on the nature of the nematic state of the pnictides, our approach provides a novel route to investigate electronic nematicity in other strongly correlated systems where this type of state has been proposed.

We thank F. Rullier-Albenque for providing us with transport data. We acknowledge fruitful discussions with A. Chubukov, V. Keppens, D. Mandrus and J. Schmalian. Y. G., L. C., Y.-X. Y., M. C., M.-A. M., A. S., D. C. and A. F. acknowledge support from Agence Nationale de la Recherche through Grant PNICTIDES.

*yann.gallais@univ-paris-diderot.fr

[1] S. A. Kivelson, E. Fradkin, and V. J. Emery, Nature (London) **393**, 550 (1998).
[2] M. P. Lilly, K. B. Cooper, J. P. Eisenstein, L. N. Pfeiffer, and K. W. West, Phys. Rev. Lett. **82**, 394 (1999).

[3] S. A. Kivelson, I. P. Blindloss, E. Fradkin, V. Oganesyan, J. M. Tranquada, A. Kapitulnik, and C. Howald, Rev. Mod. Phys. **75**, 1201 (2003).
[4] R. Daou, J. Chang, D. LeBoeuf, O. Cyr-Choiniére, F. Laliberté, N. Doiron-Leyraud, B. J. Ramshaw, R. Liang, D. A. Bonn, W. N. Hardy, and L. Taillefer, Nature (London) **463**, 519 (2010).
[5] R. A. Borzi, S. A. Grigera, J. Farrell, S. J. S. Lister, S. L. Lee, D. A. Tennant, Y. Maeno, and A. P. Mckenzie, Science **315**, 214 (2007).
[6] R. Okazaki, T. Shibauchi, H. J. Shi, Y. Haga, T. D. Matsuda, E. Yamamoto, Y. Onuki, H. Ikeda, and Y. Mastuda, Science **331**, 439 (2011).
[7] J.-H. Chu, J. G. Analytis, K. De Greve, P. L. McMahon, Z. Islam, and Y. Yamamoto, Science **329**, 824 (2010).
[8] S. Kasahara, H. J. Shi, K. Hashimoto, S. Tonegawa, Y. Mizukami, T. Shibauchi, K. Sugimoto, T. Fukuda, T. Terashima, A. H. Nevidomskyy, and Y. Matsuda, Nature (London) **486**, 382 (2012).
[9] M. A. Tanatar, E. C. Blomberg, A. Kreyssig, M. G. Kim, N. Ni, A. Thaler, S. L. Bud'ko, P. C. Canfield, A. I. Goldman, I. I. Mazin, and R. Prozorov, Phys. Rev. B **81**, 184508 (2010).
[10] T. M. Chuang, M. P. Allan, J. Lee, Y. Xie, N. Ni, S. L. Bud'ko, G. S. Boebinger, P. C. Canfield, and J. C. Davis, Science **327**, 181 (2010).
[11] J.-H. Chu, H.-H. Kuo, J. G. Analytis, and I. R. Fisher, Science **337**, 710 (2012).
[12] M. Yi, D. Lu, J.-H. Chu, J. G. Analytis, A. P. Sorini, A. F. Kemper, B. Moritz, S.-K. Mo, R. G. Moore, M. Hasimoto, W.-S. Lee, Z. Hussain, T. P. Devereaux, I. R. Fisher, and Z.-X. Shen, Proc. Natl. Acad. Sci. U.S.A. **108**, 6878 (2011).
[13] A. Dusza, A. Lucarelli, F. Pfuner, J.-H. Chu, I. R. Fisher, and L. Degiorgi, Europhys. Lett. **93**, 37 002 (2011).
[14] C. Fang, H. Yao, W.-F. Tsai, J.-P. Hu, and S. A. Kivelson, Phys. Rev. B **77**, 224509 (2008).
[15] C. Xu, M. Muller, and S. Sachdev, Phys. Rev. B **78**, 020501 (2008).
[16] R. M. Fernandes, A. V. Chubukov, J. Knolle, I. Eremin, and J. Schmalian, Phys. Rev. B **85**, 024534 (2012).
[17] I. Paul, Phys. Rev. Lett. **107**, 047004 (2011).
[18] C. C. Lee, W.-G. Yin, and W. Ku, Phys. Rev. Lett. **103**, 267001 (2009).
[19] C. C. Chen, J. Maciejko, A. P. Sorini, B. Moritz, R. R. P. Singh, and T. P. Devereaux, Phys. Rev. B **82**, 100504 (2010).
[20] W. Lv, F. Kruger, and P. Phillips, Phys. Rev. B **82**, 045125 (2010).
[21] S. Onari and H. Kontani, Phys. Rev. Lett. **109**, 137001 (2012).
[22] R. M. Fernandes and J. Schmalian, Supercond. Sci. Technol. **25**, 084005 (2012).
[23] See Supplemental Material at http://link.aps.org/supplemental/10.1103/PhysRevLett.111.267001 for explicit expressions for the Raman form factors.
[24] See Supplemental Material at http://link.aps.org/supplemental/10.1103/PhysRevLett.111.267001 for details about the Raman experiments and the extraction of the static nematic charge susceptibility.
[25] L. Chauvière, Y. Gallais, M.-A. Méasson, M. Cazayous, A. Sacuto, D. Colson, and A. Forget, Phys. Rev. B **84**, 104508 (2011).
[26] F. Rullier-Albenque, D. Colson, A. Forget, and H. Alloul, Phys. Rev. Lett. **103**, 057001 (2009).
[27] T. P. Devereaux and R. Hackl, Rev. Mod. Phys. **79**, 175 (2007).
[28] L. Tassini, F. Venturini, Q.-M. Zhang, R. Hackl, N. Kikugawa, and T. Fujita, Phys. Rev. Lett. **95** 117002 (2005).
[29] H. Yamase and R. Zeyher, Phys. Rev. B **83**, 115116 (2011); Phys. Rev. B **88**, 125120 (2013).
[30] See Supplemental Material at http://link.aps.org/supplemental/10.1103/PhysRevLett.111.267001 for an analysis of the functional form of the quasielastic peak.
[31] R. M. Fernandes, L. H. VanBebber, S. Bhattacharya, P. Chandra, V. Keppens, D. Mandrus, M. A. McGuire, B. C. Sales, A. S. Sefat, and J. Schmalian, Phys. Rev. Lett. **105**, 157003 (2010).
[32] M. Yoshizawa, D. Kimura, T. Chiba, S. Simayi, Y. Nakanishi, K. Kihou, C.-H. Lee, A. Iyo, H. Eisaki, M. Nakajima, and S. Uchida, J. Phys. Soc. Jpn. **81**, 024604 (2012).
[33] B. Valenzuela, M. J. Calderón, G. León, and E. Bascones, Phys. Rev. B **87**, 075136 (2013).
[34] See Supplemental Material at http://link.aps.org/supplemental/10.1103/PhysRevLett.111.267001 for the correspondence between charge nematic and orbital fluctuations in iron-pnictides.
[35] H. Yamase and R. Zeyher, Phys. Rev. B **88**, 180502(R) (2013).
[36] G. Blumberg, P. Littlewood, A. Gozar, B. S. Dennis, N. Motoyama, H. Eisaki, and S. Uchida, Science **297**, 584 (2002).